CrystEngComm

Accepted Manuscript

ROYAL SOCIETY OF CHEMISTRY

www.rsc.org/crystengcomm

Facile fabrication of urchin-like hollow boehmite and alumina microspheres with hierarchical structure via Triton X-100 assisted hydrothermal synthesis

Huihui Huang[a], Lei Wang[a,*], Yuan Cai[a,b], Caicheng Zhou[a], Yuewei Yuan[a], Xiaojun Zhang[a], Hui Wan[a], Guofeng Guan[a,*]

[a] *College of Chemistry and Chemical Engineering and State Key Laboratory of Materials-Oriented Chemical Engineering, Nanjing Tech University, Nanjing 210009, P. R. China*

[b] *Department of Chemical Engineering, Nanjing College of Chemical Technology, Nanjing 210048, P. R. China*

*Corresponding author, telephone: +86-25-83587198

E-mail: wanglei@njtech.edu.cn, guangf@njtech.edu.cn

KEYWORDS: boehmite; alumina; hierarchical; urchin-like; hollow microspheres; Triton X-100

ABSTRACT

Hierarchically organized urchin-like hollow boehmite and alumina microspheres were successfully synthesized via facile *tert*-octyl-phenyl polyoxyethylene ether (Triton X-100) assisted hydrothermal route using aluminum sulfate and urea as aluminum source and precipitant, respectively. The samples were characterized by X-ray diffraction (XRD), thermogravimetry (TG), Fourier transform infrared spectroscopy (FT-IR), scanning electron microscopy (SEM), transmission electron microscopy (TEM) and N_2 adsorption-desorption technique. SEM and TEM verified the hierarchically organized urchin-like hollow structure of the as-prepared samples with needles of about 1 μm length. The morphology and textual structure of boehmite and alumina can be handily controlled by adjusting the concentration of Triton X-100. Urchin-like alumina with large S_{BET} value of 146.91 m^2/g, pore volume of 0.92 cm^3/g and hierarchical structure was obtained at C_{TX}=0.01 M. Furthermore, a possible mechanism was also proposed for the formation of this hierarchically organized urchin-like boehmite.

Introduction

In the last decade, the design and synthesis of hollow micro-/nano-spheres with hierarchical structure have still been of widespread interests and applied in various fields[1-5] for their distinctive characteristics[6, 7], including low density, high specific surface area, large void fraction, low thermal expansion, refractive index, etc. Among diverse materials, boehmite (γ-AlOOH) and alumina are important industrial materials and have been widely used as adsorbents, ceramics, abrasives, catalysts and catalyst supports[8-11] taking [11]advantage of their unique physicochemical properties. Accordingly, the potential applications impel researchers to design and fabricate boehmite and alumina with novel morphologies and structures. In previous studies, diversified morphologies of hierarchical boehmite, such as hollow spheres with nanoflake-like surface[12, 13], flower-like 3D boehmite formed of nanostrips[14], flower-like structure composed of needle-like building blocks[15], flower-like hierarchical γ-AlOOH with thin lamellar structures[16], core/shell microspheres[17], self-encapsulated and hollow architectures with nano-flakelets[18] and so on. Although the existing approaches are effective to prepare boehmite and alumina with various hierarchical structures, it remains a challenge to develop a facile and environmentally friendly method for fabrication of hierarchical hollow boehmite and alumina with novel building blocks.

Among various synthetic methods, the template-assisted method has been proved to be an effective approach to fabricate different kinds of metal oxides with hierarchical structure[19]. Triton X-100 (*tert*-octyl-phenyl polyoxyethylene ether, TX-100 for short) is a kind of nonionic surfactant with features of low cost and biodegradability, which can

be regarded as "green" alternative surfactant. Rather, the most important advantage of TX-100 is that, compared with polyethylene glycol (PEG), it possesses not only a hydrophilic polyethylene oxide group (-CH_2-CH_2-O-), but also a bulk *tert*-octyl-phenyl hydrophobic group. When TX-100 is used as a template, it may lead to inorganic materials with interesting morphologies and structures, and create distinct porous structure[20] owing to the bulk hydrophobic group.

Herein, we report a facile and environmentally friendly method for hydrothermal synthesis of urchin-like boehmite hollow microspheres using TX-100 as surfactant. The boehmite precursors were converted to alumina with well-preserved morphologies after calcination. The effects of TX-100 on morphology and textual structure of boehmite and alumina were investigated in detail. Furthermore, based on related experiments and characterization results, a possible formation mechanism of urchin-like hollow boehmite microspheres was also proposed.

Results and discussion

Structure property and morphology

Powder XRD is used to monitor the phase structure of samples. Figure 1 (A) shows the wide-angle XRD patterns of samples synthesized at C_{TX} =0.065 M before and after calcination. All sharp diffraction peaks can be indexed to the orthorhombic boehmite (γ-AlOOH) (JCPDS No. 21-1307), demonstrating well-crystallized and high purity γ-AlOOH is formed. The broaden diffraction peaks indicate boehmite is composed of small crystals in nanoscale. After calcination at 800 ^oC for 6 h, the XRD patterns of alumina obtained are mainly indexed as the diffractions of γ-Al_2O_3 (JCPDS No.

10-0425) with little δ-Al_2O_3 (JCPDS No. 04-0877). The weak intensity and broad bands indicate the low crystallinity of resulting alumina.

The decomposition of as-synthesized sample upon heat treatment could help to understand the conversion process of precursors. Figure 2 presents the TGA-DTG curves of the typical γ-AlOOH synthesized at C_{TX}=0.065 M. The endothermic peak below 200 ^oC corresponds to the removal of physically adsorbed water. The second mass loss (16 wt%) ranged from 200 ^oC to 520 ^oC with a sharp asymmetric endothermic peak at ~390 ^oC can be mainly associated with the removal of hydroxyl group in γ-AlOOH. However, the theoretical weight loss of the phase transition from boehmite to alumina is 15 wt%, which means the actual weight loss is higher than the theoretical value. The extra mass loss (1 wt%) can be ascribed to the decomposition of TX-100[21]. This confirms some TX-100 occluded in boehmite although no typical peaks of TX-100 in its corresponding XRD patterns are observed. Mass loss continues to occur above 520 ^oC. The slight endothermic peak around 600 °C is ascribed to the further dehydroxylation of γ-Al_2O_3[22, 23]. The weight loss caused by the decomposition of sulfate ions is observed from 650 °C[24]. The last mass loss with an endothermic peak centered at ~785 ^oC corresponds to the formation of δ-Al_2O_3[25]. The transformation of boehmite to alumina is in agreement with the XRD results of obtained alumina by calcination at different temperatures, as shown in Figure 1(B).

To further ascertain the chemical compositions of boehmite and alumina, FT-IR measurement is carried out in the region of 400-4000 cm^{-1}. The typical FT-IR spectra of pure TX-100, boehmite and alumina synthesized at C_{TX}=0.065 M are shown in Figure 3.

The FT-IR spectrum of pure TX-100 is in agreement with literatures[26, 27]. In the FT-IR spectrum of boehmite, the adsorption bands at 3319, 3100, 1640, 1368, 1147, 1068, 750, 628 and 480 cm^{-1} are typical features of γ-AlOOH[28-30], which are consistent with XRD results. The weak bands at 2949, 2866, 1511, 1244 cm^{-1} ascribed to the characteristic groups of TX-100 are detectable. Meanwhile, trace amount of TX-100 still exists in γ-AlOOH though the sample has been washed for several times. This phenomenon can be related to the hydrogen bond between TX-100 and -OH in γ-AlOOH. After calcination, the bands at 3466, 1640, 798, 543 cm^{-1} are consistent with the reported value of γ-Al_2O_3[31, 32]. The characteristics peaks of δ-Al_2O_3 are not detected in the spectrum of alumina, possibly owing to trace amount of it. The characteristic groups of TX-100 disappeared, indicating TX-100 had been removed after thermal treatment, which is in accord with the results of TGA-DTG.

SEM and TEM images of the as-synthesized γ-AlOOH and alumina synthesized at C_{TX}=0.065 M are shown in Figure 4. γ-AlOOH are urchin-like microspheres assembled by interconnected needle-like building blocks which are originated from the same core and aligned perpendicularly to the spherical surface. The mean diameter of urchin-like microspheres is about 2-3 μm with needles length about 1 μm. The needles are made up of nanocrystals with nanometer-sized holes inside (inset image in Figure 4 (d)), which may contribute to high specific surface area and pore volume. The shell thickness of microspheres is about 200-300 nm, and the inside hollow structures can be obviously observed from the broken microspheres and high-magnification TEM image in Figure 4 (d, e). Notably, the urchin-like hollow microspheres are stable, even after sonication and

calcination under 800 ^{o}C, as shown in SEM/TEM images of alumina (Figure 4 (c, f)).

Figure 5 exhibits N_2 adsorption-desorption isotherm and pore-size distribution (inset) of alumina synthesized at C_{TX}=0.065 M. The isotherm is type IV according to the International Union of Pure and Applied Chemistry (IUPAC) classification[33]. When the relative pressure is between 0.4 and 1, the isotherm exhibits H2 and H3 hysteresis loops, suggesting a multi-modal pore-size distribution in the mesoporous and macroporous region[34, 35]. This type of distribution can be found in solids composed of aggregates or agglomerates of particles[36], which is consistent with the presence of the needle-like building blocks composed of small crystals, as illustrated by TEM. The pore structure parameters of alumina are listed in Table 1. The sample has a high specific surface area, large pore volume and hierarchical pore size. As observed from the BJH pore-size distribution curves, the major mesopore size distribution centers at 3, 12, 20 nm and the macroporous distribution centers at ~60 nm. In detail, the small pores presumably arise from the inter-needle spaces, the middle pores are possibly attributed to the voids of needles and large pores may be caused by hollow structures.

Effect of TX-100 concentration

To understand the role of TX-100 in the formation of this urchin-like microspheres assembled by needle-like building blocks, XRD, TG, SEM and N_2 adsorption-desorption are used to monitor the effect of TX-100 concentration. Compared with γ-AlOOH synthesized in the presence of TX-100, the intensities of XRD peaks of that without TX-100 are weaker, as shown in Figure 6. Therefore, the addition of TX-100 facilitates the crystallization of γ-AlOOH. What's more, the relative

intensity of precursors synthesized with TX-100 firstly increases and then decreases by varying the concentration of TX-100 from 0.008 through 0.03 M to 0.13 M, the crystallinity also changes at the same trend with increasing concentration of TX-100. All alumina obtained by calcination at 800 ^{o}C for 6 h are mainly indexed as the diffractions of γ-Al_2O_3 (JCPDS No. 10-0425) with little δ-Al_2O_3 (JCPDS No. 04-0877) (Figure S1).

From the TG curves (Figure S3) of γ-AlOOH synthesized at varying concentration of TX-100, the weight loss of γ-AlOOH synthesized at C_{TX}=0.03, 0.065 M between 200 ^{o}C and 600 ^{o}C is more than that synthesized without TX-100, while that of γ-AlOOH synthesized at C_{TX}=0.10, 0.13 M is less. This result could be explained as that the oxygen atoms of the PEO chain in TX-100 interact with the -OH of γ-AlOOH layers by hydrogen bonds to squeeze out part of structural water[37, 38]. When the residual TX-100 in γ-AlOOH is more than the squeeze-out water, so the weight loss is more, as γ-AlOOH synthesized at C_{TX}=0.10, 0.13 M.

Without TX-100, γ-AlOOH (Figure S4 (a)) consists mainly of randomly incompact stacks of needle-like particles. However, the morphology of γ-AlOOH turns to be urchin-like microspheres when synthesized in the presence of TX-100. Namely, TX-100 plays a vital role in the formation of urchin-like microspheres. However, varying the amount of TX-100 from 0.008 to 0.13 M only has minor effect on the morphology of γ-AlOOH that displays a slightly longer needle texture, and the morphology of urchin-like hollow microspheres are well preserved after thermal treatment of γ-AlOOH at 800 ^{o}C.

The effect of TX-100 on textual structure of alumina is analyzed by N_2 adsorption-desorption. Figure 7 presents the adsorption-desorption isotherms and BJH pore-size distribution. The type IV isotherms exhibit H2 and H3 hysteresis loops. The pore structure parameters of all alumina are listed in Table 1. All samples have high specific surface areas, large pore volume and hierarchical pore size. As observed from the BJH pore-size distribution curves (Figure 7 (B)), the major mesopore size distribution centers at 10-15 nm, 25-30 nm and the macroporous distribution centers at ~80 nm. Alumina microspheres with large S_{BET} value of 146.91 m^2/g, pore volume of 0.92 cm^3/g and hierarchical pore size are obtained at C_{TX}=0.01 M. It is worth noting that the pore volumes and average pore sizes of aluminas change markedly along with the amount of TX-100, indicating the effect of TX-100 on the textural structure of alumina is significant. The pore volumes of all alumina synthesized with TX-100 are larger than that without TX-100. The pore volume also increases firstly and then decreases, approximately following a linear relationship with increasing concentration of TX-100, as shown in Figure S5. As it is known, the layers of boehmite are formed by Al^{3+} octahedrally surrounded by O^{2-} and OH^-, which are linked by hydrogen bonds. The surfactant would be located in the interlayer space[39, 40], the oxygen atoms of the PEO chain in TX-100 interacting with the -OH of boehmite layers by hydrogen bonds. In addition, alkylene oxide segments can form crown-ether-type complexes with many inorganic ions through weak coordination bonds[41]. The PEO-aluminum complexation interactions also play a part in the mesostructure formation. At the same time, the bulk hydrophobic groups will hinder the particles from aggregating. In consequence, the

mesostructure would take place upon calcination. At high C_{TX}, excess surfactant may not be able to access or link to boehmite surface, so excess surfactant existed in the intercrystallite voids would act as space filler resulting in increased pore structure. As reported in previous work[39], the role of Triton X-114 in building-up the pore network of the calcined materials is also significant. Therefore, the textual structure of alumina can be handily controlled by adjusting the concentration of TX-100.

The above results provide a facile hydrothermal method for synthesis of urchin-like boehmite and alumina hollow microspheres, which are composed of hierarchical structures: i) boehmite crystals at nanoscale, ii) needle-like building blocks composed of numerous boehmite crystals and iii) the hollow internal cavity. In comparison with solid particles of similar size, these urchin-like porous alumina hollow microspheres possess both outer and interior void space, which can be used to accommodate a large amount of guest molecules or species of different sizes. These structural features of urchin-like hollow alumina microspheres studied make them promising in areas[42] such as shape selective catalysis, adsorption, gas separation and biomedical applications.

Growth mechanism of urchin-like hollow γ-AlOOH microspheres with hierarchical structure

To investigate the growth mechanism of as-synthesized urchin-like γ-AlOOH hollow microspheres, time-dependent experiments were conducted at C_{TX}=0.065 M. TEM and XRD are employed to monitor the evolution of morphology and crystalline structure of as-synthesized samples with time, as shown in Figure 8. No precipitates

were observed when the mixed solution reacted at 120 ^{o}C for 2 h. After reaction for 3 h, amorphous spherical aluminum hydroxide particles aggregated to form solid spheres with a diameter of 1-2 μm. After 6 h, γ-AlOOH microspheres, with short and not well developed needles aligned perpendicularly to the surface of the microspheres, were obtained. By extending the hydrothermal time to 12 h or 18 h, along with increase in the length and number of needles, the dissolution of γ-AlOOH solid core brought about core/shell microspheres. Further prolonging the reaction time to 24 h resulted in the formation of hollow microspheres consisted of quantities of needles with length of about 1 μm. The similar formation process can also be found in BiOI and ZnO systems[43, 44]. The crystallization of the as-prepared samples also improved as illustrated by the increase in the intensities of XRD diffraction peaks.

Based on the above results, a possible formation mechanism of urchin-like hollow microspheres γ-AlOOH is proposed as shown in Scheme 1. The mechanism may be related to chemically induced self-transformation[45]. Before the hydrothermal reaction, pH value of the clear mixed solution is only 3. When the mixed solution is heated at 120 ^{o}C, urea begins to hydrolyze and undergo slow evolution of ammonia[46]. Then OH^- is generated by the hydrolysis of ammonia, causing a gradual increase of pH. When pH reaches 4.2[46], precipitation of amorphous aluminum hydroxide occurs by a polycondensation reaction of Al^{3+} and OH^-. In aqueous solution, spherical micelles of TX-100 are generated and the overall radius of TX-100 micelle is about 51 Å[47]. The TX-100 micelles interacted with particles via hydrogen bond, electrostatics and van der Waals force[48], resulting in spherical particles with a diameter of ~5 nm, as shown in the

inset image in Figure 8 (a). The spherical particles subsequently aggregate to solid spheres with a diameter of 1-2 μm. The microspheres grow continuously and start to crystalize, as a result, the size of particles at the surface becomes larger and their crystallinity becomes better. Meanwhile, TX-100 takes the layers of boehmite in, whose oxygen atoms of hydrophilic poly(ethylene oxide) (PEO) chain interact with the OH group of boehmite crystallites by hydrogen bonds, while the alkyl chains head away from the surface[49] and facilitate the transportation of aluminum ions to boehmite crystal plane (020)[50], which can be clearly seen from the XRD pattern of γ-AlOOH synthesized in the presence of TX-100. In this way, the surface energy of crystallites reduces and the lateral surface of particles is passivated by PEO chain[51]. Consequently, the boehmite crystallites on the exterior surface of microspheres grow along the direction perpendicular to spherical surface, which convert nanoparticles to thermodynamically more stable needles, as shown in Figure 8 (c). As the reaction proceeds, γ-AlOOH microspheres conduct the dissolution-recrystallization process. Compared with the particles on the surface of microspheres, the inner amorphous small particles have higher surface energy, which provides the driving force for the in-side out Ostwald ripening[52-54]. Thus, the inside particles of microspheres start to be evacuated through dissolution of γ-AlOOH solid core, and then recrystallize at the exterior of the microspheres with an increase of OH^- concentration by prolonging the reaction time, resulting in core/shell microspheres. The hollow degree of γ-AlOOH microspheres further develops until the entire formation of hollow urchin-like superstructure.

Conclusions

In conclusion, the hierarchically boehmite and alumina urchin-like hollow microspheres with interconnected needle-like building blocks have been successfully synthesized by TX-100 assisted hydrothermal method. All boehmite synthesized with TX-100 are urchin-like hollow microspheres composed of numerous needle-like building blocks. What's more, the morphology and structure of boehmite are significantly influenced by the concentration of TX-100. The urchin-like hollow microspheres of boehmite have a diameter of 2-3 μm, the mean length of needle-like building blocks is around 1 μm. The morphology of boehmite could be well preserved after calcination and the alumina with hierarchically urchin-like hollow microspheres structure are observed. The pore volume and average pore size of alumina can be controlled by adjusting the concentration of TX-100. Alumina microspheres with large S_{BET} value of 146.91 m^2/g, pore volume of 0.92 cm^3/g and hierarchical pore size are obtained at C_{TX}=0.01 M. Based on time dependent experiments, chemically induced self-transformation mechanism for the formation of hierarchically organized boehmite urchin-like hollow microspheres is proposed. The hierarchical features of the prepared boehmite and alumina make them promising in areas such as shape selective catalysis, adsorption, gas separation and biomedical applications.

Experimental

Synthesis of boehmite and alumina. All reagents were of analytical grade and used as received without further purification. The boehmite precursors were synthesized by TX-100 assisted hydrothermal precipitation reaction of $Al_2(SO_4)_3 \cdot 18H_2O$ and urea.

In a typical synthesis, 3.3 g $Al_2(SO_4)_3$ •$18H_2O$, 7.2 g urea and a certain amount of TX-100 were dissolved in 100 ml deionized water to form a mixed solution under vigorous stirring. Then the clear solution was transferred into a Teflon-lined autoclave and heated at 120 ^oC. Afterwards, the resulting white precipitates were washed with deionized water and anhydrous ethanol, and then dried at 60 ^oC overnight. The as-synthesized precursors were calcined at 800 ^oC for 6 h to get corresponding alumina. Similar experiments were performed by varying concentration of TX-100 (C_{TX}) from 0 to 0.13 M and reaction time from 2 to 24 h.

Characterization. The XRD was performed on a Philips X'pert MPD Pro diffractometer equipped with Ni-filtered Cu Kα radiation (λ=0.15418 nm). The X-ray tube was operated at 40 kV and 100 mA. The scanning angle was from 5º to 75º with a scan-step of 0.02º per second. The thermogravimetric (TG) were conducted with use of a Netzsch STA 449F3 TG thermogravimetric analyzer. Samples of approximately 5 mg were heated up to 800 ^oC in air flow with a heating rate of 10 ^oC/min. FT-IR spectra were collected on a Thermo Nicolet 870 spectrophotometer with a resolution of 5 cm^{-1} using anhydrous KBr as dispersing agent. Scanning Electron Microscopy (SEM) was taken on a Hitachi S4800 field-emission SEM instrument at 5 kV. TEM images were obtained with a JEOL (model 794) instrument employing an acceleration voltage of 120 kV. The samples were daubed onto carbon film supported on copper grids after sonicating in ethanol for 15 min. N_2 adsorption-desorption measurements were carried out on a Micromeritics ASAP 2020 system model instrument at 77 K. The specific surface area was calculated by Brunauer-Emmett-Teller (BET) algorithm. The

mesoporous pore size distribution was obtained through the Barrett-Joyner-Halenda (BJH) theory.

Acknowledgement

This work was financially supported by National Natural Science Foundation of China (Grant No. 21306082), Natural Science Foundation of the Jiangsu Higher Education Institutions of China (12KJB530004), and the Foundation from State Key Laboratory of Materials-Oriented Chemical Engineering, Nanjing Tech University (ZK201305).

References

1. J.-H. Lee, *Sensor Actuat B: Chemical*, 2009, 140, 319-336.
2. J. F. Chen, H. M. Ding, J. X. Wang and L. Shao, *Biomaterials*, 2004, 25, 723-727.
3. C. K. King'ondu, A. Iyer, E. C. Njagi, N. Opembe, H. Genuino, H. Huang, R. A. Ristau and S. L. Suib, *J. Am. Chem. Soc.*, 2011, 133, 4186-4189.
4. X. Lai, J. E. Halpert and D. Wang, *Energ. Environ. Sci.*, 2012, 5, 5604-5618.
5. S. Simonato, H. Groger, J. Mollmer, R. Staudt, A. Puls, F. Dreisbach and C. Feldmann, *Chem. Commun.*, 2012, 48, 844-846.
6. X. W. Lou, L. A. Archer and Z. C. Yang, *Adv. Mater.*, 2008, 20, 3987-4019.
7. J. Hu, M. Chen, X. Fang and L. Wu, *Chem. Soc. Rev.*, 2011, 40, 5472-5491.
8. N. Nagai, K. Ihara, A. Itoi, T. Kodaira, H. Takashima, Y. Hakuta, K. K. Bando, N. Itoh and F. Mizukami, *J. Mater. Chem.*, 2012, 22, 21225-21231.
9. K. V. P. M. Shafi, A. Ulman, J. Lai, N.-L. Yang and M.-H. Cui, *J. Am. Chem.*

Soc., 2003, 125, 4010-4011.

10. G. Paglia, E. S. Božin and S. J. L. Billinge, *Chem. Mater.*, 2006, 18, 3242-3248.
11. L. H. Nie, A. Y. Meng, J. G. Yu and M. Jaroniec, *Sci. Rep.*, 2013, 3, 3215-3220.
12. Z. Tang, Y. Liu, G. Li, X. Hu and C. Liu, *Mater. Res. Bull.*, 2012, 47, 3177-3184.
13. W. Q. Cai, S. G. Chen, J. G. Yu, Y. Z. Hu, C. X. Dang and S. H. Ma, *Mater. Chem. Phys.*, 2013, 138, 167-173.
14. J. Zhang, S. J. Liu, J. Lin, H. S. Song, J. J. Luo, E. M. Elssfah, E. Ammar, Y. Huang, X. X. Ding, J. M. Gao, S. R. Qi and C. C. Tang, *J. Phys. Chem. B*, 2006, 110, 14249-14252.
15. Y. H. Li, C. Peng, L. L. Li and P. G. Rao, *J. Am. Ceram. Soc.*, 2014, 97, 35-39.
16. Y. X. Zhang, Y. Jia, Z. Jin, X. Y. Yu, W. H. Xu, T. Luo, B. J. Zhu, J. H. Liu and X. J. Huang, *CrystEngComm*, 2012, 14, 3005-3007.
17. L. M. Zhang, W. C. Lu, L. M. Yan, Y. L. Feng, X. H. Bao, J. P. Ni, X. F. Shang and Y. Lv, *Micropor. Mesopor. Mat.*, 2009, 119, 208-216.
18. X. Wu, D. Wang, Z. Hu and G. Gu, *Mater. Chem. Phys.*, 2008, 109, 560-564.
19. J. M. Patete, X. H. Peng, C. Koenigsmann, Y. Xu, B. Karn and S. S. Wong, *Green Chem.*, 2011, 13, 482-519.
20. A.-W. Xu, *J. Phys. Chem. B*, 2002, 106, 13161-13164.
21. F. Pan, X. C. Lu, T. Z. Wang, Y. Wang, Z. M. Zhang and Y. Yan, *Appl. Clay Sci.*, 2013, 85, 31-38.
22. T. C. Alex, *J. Therm. Anal. Calorim.*, 2014, 117, 163-171.
23. J. J. Fitzgerald, G. Piedra, S. F. Dec, M. Seger and G. E. Maciel, *J. Am. Chem.*

Soc., 1997, 119, 7832-7842.

24. M. N. Alaya and M. A. Rabah, *J. Alloys Compd.*, 2013, 575, 285-291.

25. X. Y. Xu, Y. X. Liu, Z. H. Li, Z. Lv, J. Q. Song, M. Y. He, Q. Wang, L. J. Yan and Z. F. Li, *J. Therm. Anal. Calorim.*, 2014, 115, 1111-1117.

26. N. Kimura, J. Umemura and S. Hayashi, *J. Colloid Interface Sci.*, 1996, 182, 356-364.

27. L. Yang, J. G. Zhu and D. Q. Xiao, *RSC Adv.*, 2012, 2, 8179-8188.

28. Y. L. Feng, W. C. Lu, L. M. Zhang, X. H. Bao, B. H. Yue, Y. Iv and X. F. Shang, *Cryst. Growth Des.*, 2008, 8, 1426-1429.

29. T. Kim, J. Lian, J. Ma, X. Duan and W. Zheng, *Cryst. Growth Des.*, 2010, 10, 2928-2933.

30. C. Xiang Ying, H. Hyun Sue and W. L. Soon, *Nanotechnology*, 2007, 18, 285608.

31. D. M. Ibrahim and Y. M. Abu-Ayana, *Mater. Chem. Phys.*, 2009, 113, 579-586.

32. K. M. Parida, A. C. Pradhan, J. Das and N. Sahu, *Mater. Chem. Phys.*, 2009, 113, 244-248.

33. K. S. W. Sing, D. H. Everett, R. A. W. Haul, L. Moscou, R. A. Pierotti, J. Rouquerol and T. Siemieniewska, *Pure Appl. Chem.*, 1985, 57, 603-619.

34. W. Q. Cai, J. G. Yu and S. Mann, *Micropor. Mesopor. Mat.*, 2009, 122, 42-47.

35. J. G. Yu, W. Liu and H. G. Yu, *Cryst. Growth Des.*, 2008, 8, 930-934.

36. M. Kruk and M. Jaroniec, *Chem. Mater.*, 2001, 13, 3169-3183.

37. A. P. Su, Y. Zhou, Y. H. Yao, C. M. Yang and H. Du, *Micropor. Mesopor. Mat.*,

2012, 159, 36-41.

38. M. Li, Z. Si, X. Wu, D. Weng and F. Kang, *J. Colloid Interface Sci.*, 2014, 417, 369-378.

39. V. González-Peña, I. Díaz, C. Márquez-Alvarez, E. Sastre and J. Pérez-Pariente, *Micropor. Mesopor. Mat.*, 2001, 44–45, 203-210.

40. M. S. Strano, V. C. Moore, M. K. Miller, M. J. Allen, E. H. Haroz, C. Kittrell, R. H. Hauge and R. E. Smalley, *J. Nanosci. Nanotechno.*, 2003, 3, 81-86.

41. P. Yang, D. Zhao, D. I. Margolese, B. F. Chmelka and G. D. Stucky, *Nature*, 1998, 396, 152-155.

42. X. Y. Yang, A. Leonard, A. Lemaire, G. Tian and B. L. Su, *Chem. Commun.*, 2011, 47, 2763-2786.

43. J. Di, J. X. Xia, Y. P. Ge, L. Xu, H. Xu, M. Q. He, Q. Zhang and H. M. Li, *J. Mater. Chem. A*, 2014, 2, 15864-15874.

44. P. Hu, X. Zhang, N. Han, W. C. Xiang, Y. B. Cao and F. L. Yuan, *Cryst. Growth Des.*, 2011, 11, 1520-1526.

45. J. G. Yu, H. Guo, S. A. Davis and S. Mann, *Adv. Funct. Mater.*, 2006, 16, 2035-2041.

46. S. Ramanathan, S. K. Roy, R. Bhat, D. D. Upadhyaya and A. R. Biswas, *Ceram. Int.*, 1997, 23, 45-53.

47. N. Nandi, K. Bhattacharyya and B. Bagchi, *Chem. Rev.*, 2000, 100, 2013-2046.

48. Q. Yuan, A. X. Yin, C. Luo, L. D. Sun, Y. W. Zhang, W. T. Duan, H. C. Liu and C. H. Yan, *J. Am. Chem. Soc.*, 2008, 130, 3465-3472.

49. H. Y. Zhu, J. D. Riches and J. C. Barry, *Chem. Mater.*, 2002, 14, 2086-2093.

50. X.-M. Wang, X.-Y. Li and K. Shih, *J. Am. Ceram. Soc.*, 2011, 94, 4435-4443.

51. J. Y. Li, S. L. Xiong, J. Pan and Y. T. Qian, *J. Phys. Chem. C*, 2010, 114, 9645-9650.

52. W. Cheng, K. Tang, Y. Qi, J. Sheng and Z. Liu, *J. Mater. Chem.*, 2010, 20, 1799-1805.

53. X. W. Lou, Y. Wang, C. Yuan, J. Y. Lee and L. A. Archer, *Adv. Mater.*, 2006, 18, 2325-2329.

54. C. C. Yec and H. C. Zeng, *J. Mater. Chem. A*, 2014, 2, 4843-4851.

Table 1. Pore structure parameters of Al_2O_3 synthesized by varying C_{TX}.

C_{TX}	Specific Surface area (m^2/g)	Pore volume (cm^3/g)	Average pore size (nm)
0	122.82	0.59	19.08
0.008	127.69	0.65	20.34
0.03	141.48	0.68	19.26
0.065	133.64	0.81	24.37
0.10	146.91	0.92	25.02
0.13	117.38	0.71	24.20

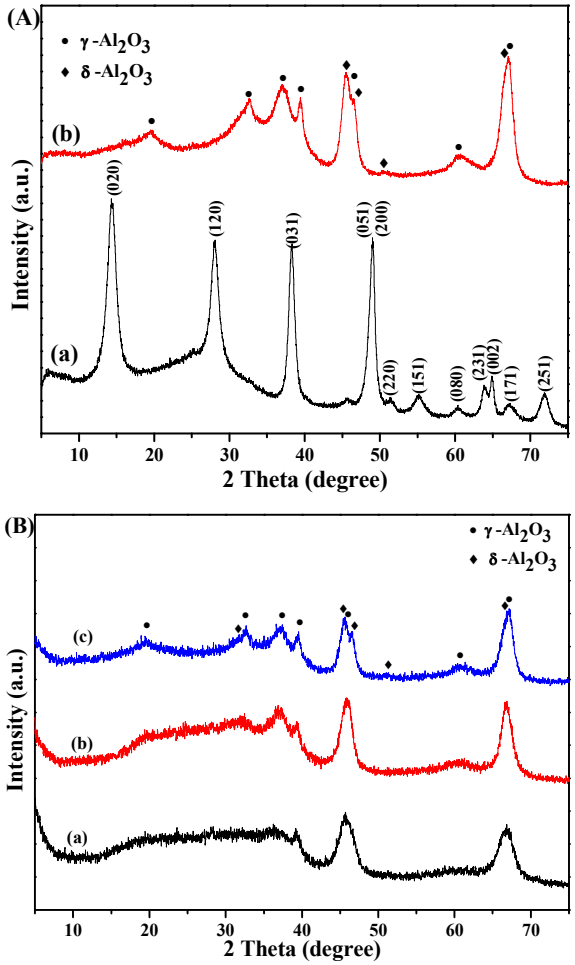

Figure 1. XRD patterns of **(A):** (a) γ-AlOOH synthesized at C_{TX}=0.065 M and (b) corresponding alumina calcined at 800 ^{o}C; **(B):** alumina obtained by calcination at 400, 600 and 800 ^{o}C for 6 h.

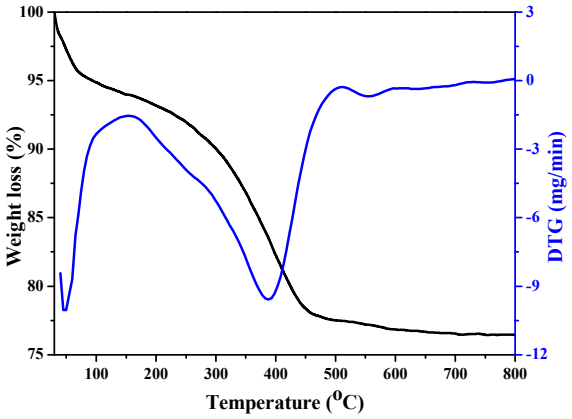

Figure 2. TGA-DTG curves of γ-AlOOH synthesized at C_{TX}=0.065 M.

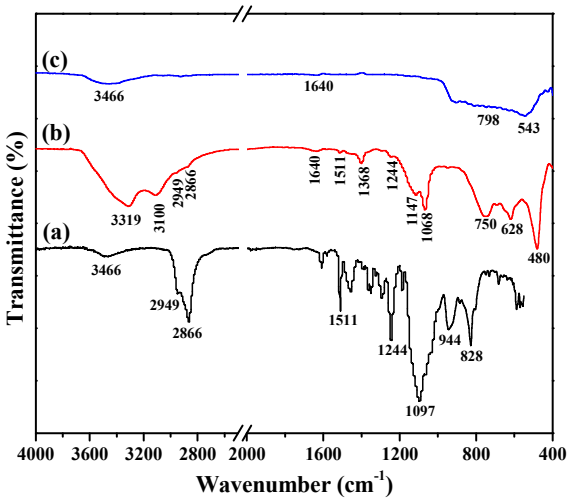

Figure 3. FT-IR spectra of (a) pure Triton X-100, (b) γ-AlOOH synthesized at C_{TX}=0.065 M and (c) corresponding alumina calcined at 800 ^{o}C.

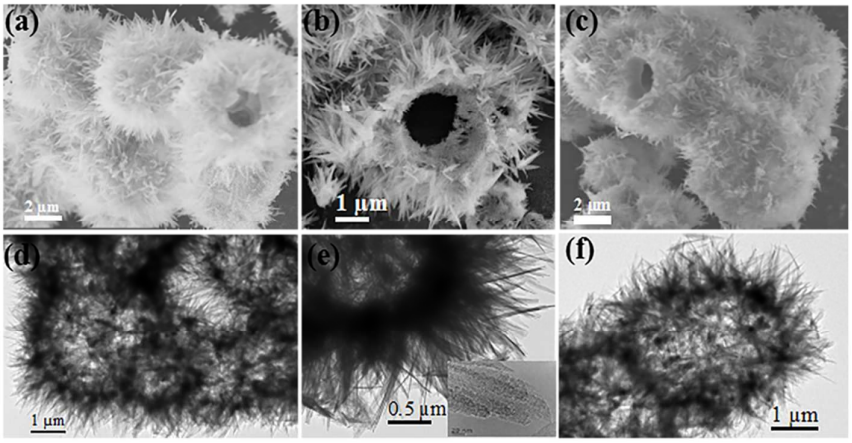

Figure 4. (a, b) SEM images and (d, e) TEM images of γ-AlOOH synthesized at C_{TX}=0.065 M and (c, f) SEM and TEM images of corresponding alumina calcined at 800 ^{o}C.

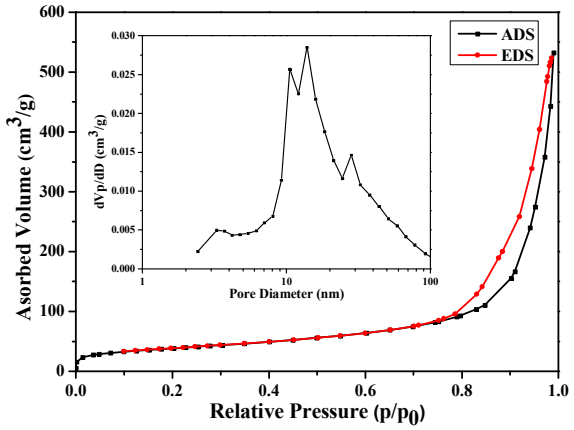

Figure 5. N_2 adsorption-desorption isotherms and corresponding pore size distributions (inset) of urchin-like hollow alumina synthesized at C_{TX}=0.065 M.

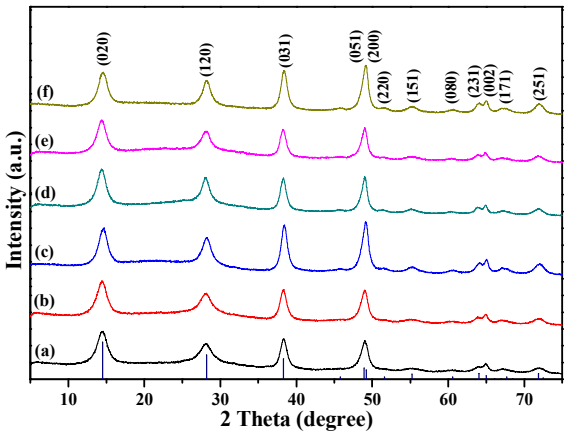

Figure 6. XRD patterns of γ-AlOOH synthesized by varying C_{TX}: (a) 0, (b) 0.008, (c) 0.03, (d) 0.065, (e) 0.1 and (f) 0.13 M.

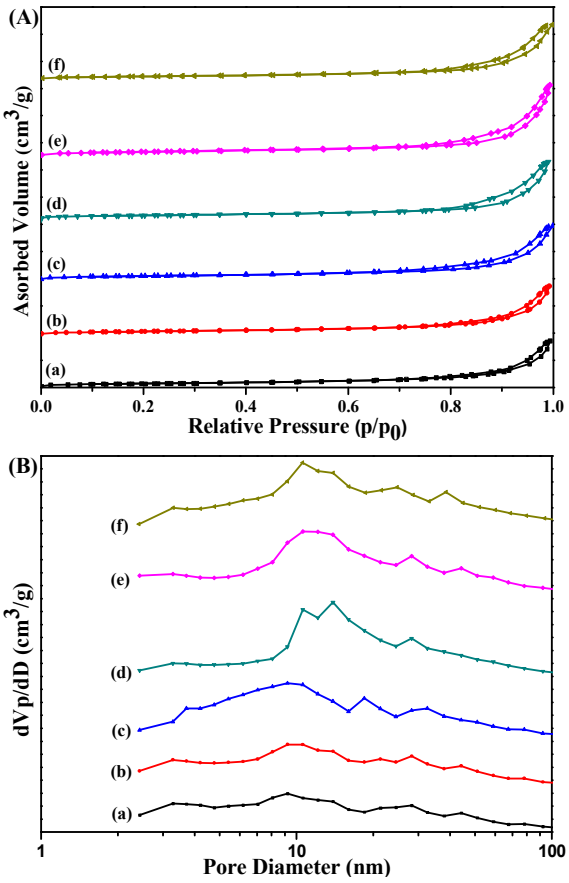

Figure 7. (A) N_2 adsorption-desorption isotherms and **(B)** pore size distributions of alumina synthesized by varying C_{TX}: (a) 0, (b) 0.008, (c) 0.03, (d) 0.065, (e) 0.1 and (f) 0.13 M.

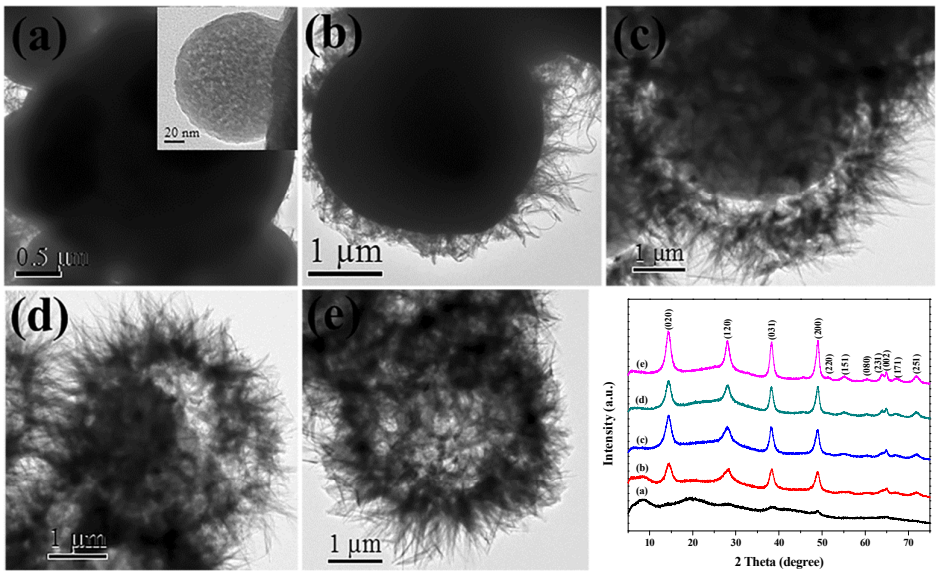

Figure 8. TEM images and XRD patterns of γ-AlOOH synthesized at C_{TX}=0.065 M for different reaction time: (a) 3 h, (b) 6 h, (c)12 h, (d)18 h, (e)24 h.

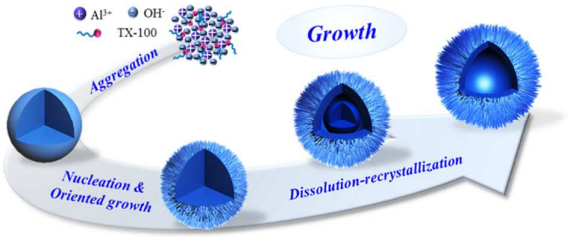

Scheme 1. Schematic illustration of the formation mechanism for urchin-like hollow γ-AlOOH microspheres with hierarchical structure.

Table of Contents entry

Facile fabrication of urchin-like hollow boehmite and alumina microspheres with hierarchical structure via Triton X-100 assisted hydrothermal synthesis

Huihui Huang[a], Lei Wang[a,*], Yuan Cai[a,b], Caicheng Zhou[a], Yuewei Yuan[a], Xiaojun Zhang[a], Hui Wan[a], Guofeng Guan[a,*]

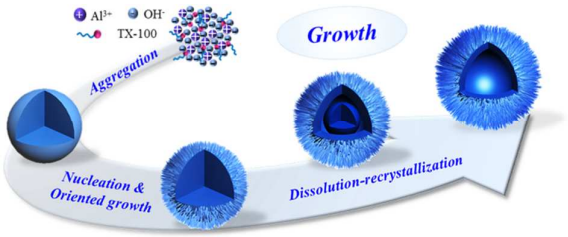

Hierarchically organized urchin-like hollow boehmite and alumina microspheres with needle-like building blocks were fabricated via *tert*-octyl-phenyl polyoxyethylene ether (Triton X-100) assisted hydrothermal synthesis.